coatings

MDPI

Article

Mechanical and Tribological Behaviors of Hot-Pressed SiC/SiC_w-Y_2O_3 Ceramics with Different Y_2O_3 Contents

Shaohua Zhang [1,2,3], Jinfang Wang [2,3], Meng Zhang [2,3], Longqi Ding [2,3], Huijun Chan [2,3], Xiyu Liu [2,3], Fengqing Wu [2,3], Zhibiao Tu [2,3], Ling Shao [2,3], Nengyong Ye [2,3], Sheng Dai [2,3], Liu Zhu [2,3,*] and Shichang Chen [1,*]

1 School of Materials Science and Engineering, Zhejiang Sci-Tech University, Hangzhou 310018, China
2 School of Materials Science and Engineering, Taizhou University, Taizhou 318000, China
3 Zhejiang Provincial Key Laboratory for Cutting Tools, Taizhou University, Taizhou 318000, China
* Correspondence: zhuliu@tzc.edu.cn (L.Z.); scchen@zstu.edu.cn (S.C.)

Abstract: Sintering additives are commonly used to reduce the conditions required for densification in composite ceramics without compromising their performances simultaneously. Herein, SiC/SiC_w-Y_2O_3 composite ceramics with 10 vol.% SiC whiskers (SiC_w) and different Y_2O_3 contents (0, 2.5, 5, 7.5, and 10 vol.%) were fabricated by hot-pressed sintering at 1800 °C, and the effects of Y_2O_3 content on the microstructure, mechanical properties, and tribological behaviors were investigated. It was found that the increased Y_2O_3 content can promote the densification of SiC/SiC_w-Y_2O_3 composite ceramics, as evidenced by compact microstructure and increased relative density. The Vickers hardness, fracture toughness, and flexural strength also increased when Y_2O_3 content increased from 2.5 vol.% to 7.5 vol.%. However, excessive Y_2O_3 (10 vol.%) aggregated around SiC and SiC_w weakens its positive effect. Furthermore, the Y_2O_3 additive also reduces the coefficient of friction (COF) of SiC/SiC_w-Y_2O_3 composite ceramics, the higher the Y_2O_3 content, the lower the COF. The wear resistance of SiC/SiC_w-Y_2O_3 composite ceramics is strongly affected by their microstructure and mechanical properties, and as-sintered SiC ceramic with 7.5 vol.% Y_2O_3 (Y075) shows the optimal wear resistance. The relative density, Vickers hardness, fracture toughness, and flexural strength of Y075 are 97.0%, 21.6 GPa, 7.7 MPa · $m^{1/2}$, and 573.2 MPa, respectively, the specific wear rate of Y075 is 11.8% of that for its competitor with 2.5 vol.% Y_2O_3.

Keywords: SiC/SiC_w-Y_2O_3 ceramics; hot-pressed sintering; Y_2O_3 additive; mechanical properties; tribological behaviors

check for updates

Citation: Zhang, S.; Wang, J.; Zhang, M.; Ding, L.; Chan, H.; Liu, X.; Wu, F.; Tu, Z.; Shao, L.; Ye, N.; et al. Mechanical and Tribological Behaviors of Hot-Pressed SiC/SiC_w-Y_2O_3 Ceramics with Different Y_2O_3 Contents. *Coatings* **2023**, *13*, 956. https://doi.org/10.3390/coatings13050956

Academic Editor: Csaba Balázsi

Received: 18 April 2023
Revised: 8 May 2023
Accepted: 15 May 2023
Published: 19 May 2023

1. Introduction

Owing to their excellent mechanical properties and abrasion resistance, silicon carbide (SiC) ceramics have been widely used in aerospace, petrochemical, and other fields [1,2]. However, the strong covalent bonding and low self-diffusion coefficient of SiC ceramics make it hard to sinter completely and get compacted microstructure [3]. Commonly, pure SiC ceramics require at least 2000 °C to get thoroughly compacted, and this considerable energy consumption should be taken seriously [1]. Besides, the high hardness of SiC also means its high brittleness, which may not be adaptable in some complex environments. Thus, it is necessary to improve the comprehensive performance of SiC ceramic against harsh work conditions.

Whisker strengthening is a very effective method to reduce the brittleness of hard ceramics. The commonly used reinforcements include SiC fibers [4], Si_3N_4 whiskers [5], SiC whiskers (SiC_w) [6–9], and others. SiC_w has better compatibility and has been widely used in the toughening study of SiC ceramics, owing to the same chemical composition and similar crystalline structure between SiC and SiC_w. SiC_w reinforcement has been used to enhance the mechanical properties, particularly the fracture toughness of SiC ceramics, due to its high elastic modulus and strength. The main toughening mechanisms

include whisker bridging, pullout, crack deflection, and their combination [6–9]. Several articles [6,7] mentioned that with SiC_w content increase, the mechanical properties of SiC ceramics increase first and then decrease. Yang et al. [8] reported that the proper content of SiC_w reinforcements could enhance the wear resistance, which was ascribed to the improved mechanical properties of SiC ceramics. However, few studies on SiC_w-reinforced SiC ceramics fabricated by hot-pressed sintering have been reported.

Recently, several articles have shown that SiC powders can be densified by incorporating sintering additives at a lower sintering temperature without compromising their performance [10–17]. Therefore, various additives like Y_2O_3 [10], La_2O_3 [11], and $RE(NO_3)_3$ [12] (RE = rare earth element), etc., as well as the combination of Al_2O_3-RE_2O_3 [13–15], AlN-RE_2O_3 [16,17], and Er_2O_3-Y_2O_3 [18] have been used in the sintering of SiC ceramics to improve its sinterability by liquid phase generation. Further, the Y_2O_3 additive has been used in various ceramics, including SiC [19–22], Si_3N_4 [23,24], TiC [25], ZrB_2-SiC [26–30], AlN-SiC [31], WC [32–34], and cordierite [35], etc. Some references [19–35] mentioned that the Y_2O_3 additive could promote the densification of the materials and influence their mechanical properties. Cheng et al. [25] presented that Y_2O_3 can improve the mechanical properties of TiC ceramics by pinning at the grain boundary. Zhang et al. [26] discovered that appropriate Y_2O_3 addition could eliminate surface oxides and suppress grain growth to promote the densification of ZrB_2-SiC ceramics. Several articles [10,19–22] reported that the Y_2O_3 additive could improve the densification of SiC ceramics at a higher sintering temperature (1900–2000 °C) to achieve excellent performance. It demonstrates that Y_2O_3 additions can accelerate the diffusion and mass transfer between the SiC matrix during sintering [12,20]. However, a much higher temperature can deteriorate the mechanical properties by vaporizing the liquid phase and generating pores [36]. Gupta et al. [37] reported that a small amount of Y_2O_3 addition could improve the mechanical and tribological properties of β-SiC ceramics. However, the preparation of SiC/SiC_w-Y_2O_3 composite ceramics and the effect of Y_2O_3 content on the mechanical and tribological properties have rarely been reported.

To obtain compact SiC ceramics at a comparatively lower sintering temperature and improve their mechanical and tribological properties simultaneously, Y_2O_3 and SiC_w are incorporated to fabricate the SiC/SiC_w-Y_2O_3 composite ceramics by hot-pressed sintering (HP) at 1800 °C. SiC_w is used as the reinforcement and kept at 10 vol.%. Y_2O_3 is the sintering additive, with content increasing from 0 to 10 vol.%. The effects of Y_2O_3 contents on the microstructure, mechanical properties, and tribological behaviors of the SiC/SiC_w-Y_2O_3 composite ceramics were investigated. This study can provide constructive suggestions and references to the field of SiC ceramic modification.

2. Experimental

2.1. Raw Powders

Alpha-SiC nanoparticles (≥99.9%, ~100 nm, Forsman, Beijing, China), β-SiC_w (≥99.9%, D0.5 μm-L12 μm, Forsman, Beijing, China), and Y_2O_3 nanoparticles (≥99.9%, ~50 nm, Aladdin, Shanghai, China) were used in this study to sinter the SiC/SiC_w-Y_2O_3 ceramics. FE-SEM (scanning electron microscopy, S-4800, HITACHI, Tokyo, Japan) images of the 3 raw powders and their XRD (X-ray diffractometer, D8 Advance, Bruker, Billerica, MA, USA) patterns are shown in Figure 1. SiC powders are irregular polygonal particles with a main crystalline structure of 6H-SiC (PDF-# 72-0018). SiC_w has a diameter of ~0.5 μm and a main crystalline structure of 3C-SiC (PDF-# 75-0254). Y_2O_3 (PDF-# 65-3178) is a subspindle floccule and agglomerated with adjacent ones. The obtained results confirmed the satisfactory morphology, size, and crystallinity of the raw powders.

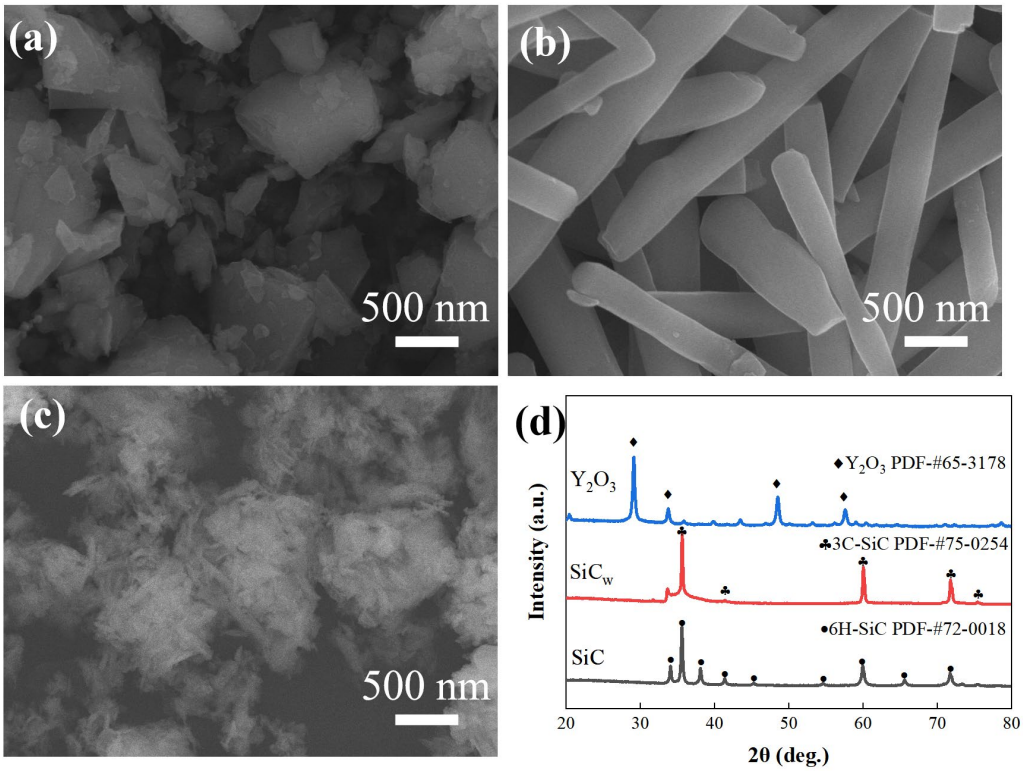

Figure 1. SEM images of (**a**) SiC powder, (**b**) SiC_w powder, (**c**) Y_2O_3 powder, and (**d**) the XRD patterns of the raw powders.

2.2. Hot-Pressed Sintering of SiC/SiC$_w$-Y$_2$O$_3$ Ceramics

To explore the effect of Y_2O_3 content on the microstructure and comprehensive properties of SiC/SiC_w-Y_2O_3 ceramics, Y_2O_3 with volume content of 0%, 2.5%, 5%, 7.5%, and 10% (denoted as Y000, Y025, Y050, Y075, and Y100, respectively) were investigated in this study. SiC_w contents were kept constant (10 vol.%), and SiC contents were in balance. The purchased powders were mixed according to their designed formula, then with ZrO_2 balls of 10 times the weight of the obtained powder and ethanol in the polyamides jar. The ball-milling of the raw powders was conducted by a planet-ball-grinding machine (MIRT-QMQX-4L, Miqi, Changsha, China), and the mill lasted without intervals for 12 h with a speed of 180 r/min. The ball-milled powders were dried, sieved, and pre-compacted in a graphite mold coated with graphite paper. Then, the green compacts were fabricated by a vacuum hot-pressed sintering furnace (ZT-40-21Y, Chenhua, Shanghai, China) to obtain SiC/SiC_w-Y_2O_3 composite ceramics with dimensions of φ26.5 mm × 6.5 mm. The sintering process was conducted at 1800 °C for 1 h under the pressure of 40 MPa in a vacuum atmosphere. The detailed sintering procedure can be found in Figure 2.

2.3. Sample Characterization

The as-sintered ceramics were polished by the diamond polishing disc and silk flannelette. The diamond spray with sizes gradually decreased to 0.25 μm was used during polishing. The specimen surfaces were finally polished to average roughness below 0.4 μm. The phase compositions of the as-sintered ceramics were detected by the mentioned XRD. Before XRD detection, the composite ceramics were carefully polished. The fracture morphologies of the composite ceramics were obtained by the three-point bending method and observed by the SEM (S-4800, HITACHI). The morphologies and chemical composition of the polished ceramics were examined by a photo-diode back-scattered electron (PDBSE) detector and an energy-dispersive X-ray spectrum (EDS, X-Max^N 20, Oxford, Oxford, UK) detector equipped on the SEM.

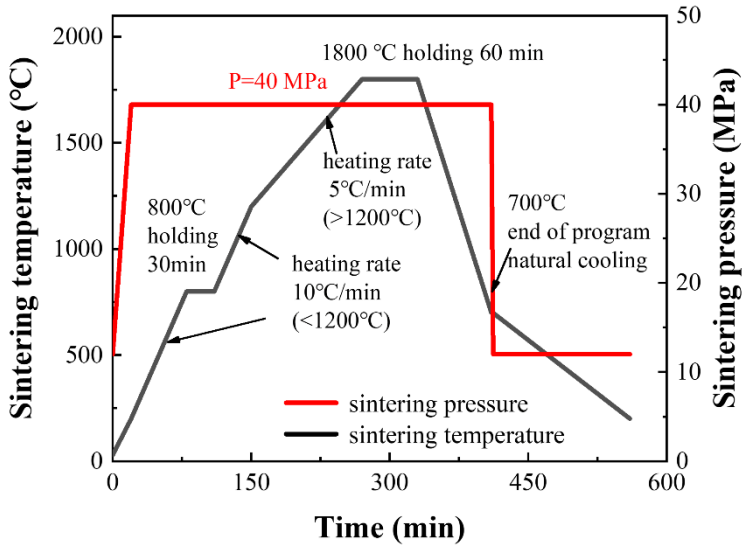

Figure 2. The schematic diagram of the sintering procedure.

2.4. Mechanical Properties

The evaluations of the mechanical properties for each group were repeated at least 5 times, and the obtained results are presented as means ± standard deviations.

2.4.1. Relative Density

Since the compactness of the as-sintered ceramics is closely related to their mechanical properties, thus, the relative density test and the corresponding results and discussion are included in the mechanical properties evaluation section. The bulk density was measured by an analytical balance (ME204, Mettler, Zurich, Switzerland) separately in air and deionized water at least 5 times, and the value of relative density (%) was calculated by the Archimedes method [11].

2.4.2. Vickers Hardness

The Vickers hardness (HV, GPa) of SiC composite ceramics with different content of Y_2O_3 was tested by a Vickers hardness tester (HV-50Z, Huayin, Laizhou, China) with a load of 20 kgf for 15 s. The length of the diagonal indentation ($2a$) and the final Vickers hardness value were obtained by the standard GB/T 4340.1-2009.

2.4.3. Fracture Toughness

The indentation fracture toughness (K_{IC}, MPa · $m^{1/2}$) of each group was obtained by the Vickers hardness tests mentioned above. The parameters, including the length of the diagonal hardness indentation ($2a$) and the crack along the edge of the indentation ($2c$), were precisely measured by the metallomicroscope (Axio Imager A2m, Zeiss, Oberkochen, Germany). Young's modulus (E) of the SiC matrix as 400 GPa was reported by Guo et al. [38]. The value of indentation fracture toughness was calculated by Equation (1) according to the Niihara [9,38,39].

$$K_{IC} = 0.0181E^{0.4}HV^{0.6}a(c-a)^{-0.5} \quad (1)$$

2.4.4. Flexural Strength

The flexural strength (σ, MPa) was investigated by a universal testing machine (CMT5305, MTS, Eden Prairie, MN, USA) with a cross-head speed of 0.2 mm/min and a span of 14.5 mm. The maximum applied load of the flexural fracture was recorded and calculated according to the 3-point bending method to obtain the value of flexural strength. Besides, the bar-shaped samples for the flexural strength test should conform to the requirement given by the standard GB/T 3851-2015 (a size of 5.5 mm × 6.25 mm × 20 mm).

2.5. Tribological Behavior

A tribometer (MFT-5000, RTEC) was used to investigate the tribological behavior of the SiC/SiC_w-Y_2O_3 composite ceramics with different Y_2O_3 contents. The specimens were polished to surface roughness below 0.4 μm before the tribological test, aiming to reduce the imperfections like scratches that would interfere with the results. The linear-reciprocating wear tests were conducted at room temperature and dry conditions with a frequency of 2 Hz, P is the applied load (20 N), sliding time of 20 min, a stroke length of 5 mm, and s is the friction stroke length (12 m). YG6 balls (6 wt.% Co, Vickers hardness: 20 GPa) with a diameter of 6.35 mm were used as friction pairs in the tests. The tribological test for each group was carried out 3 times, and the representative results were exhibited in Section 3. The coefficient of friction (COF) variation with sliding time was recorded automatically by the tribometer. The partial roughness of the worn surface can be represented by the 2D profiles and 3D morphologies characterization of the wear tracks instead of measuring the entire surface roughness after the wear test. The 2D and 3D profiles of the wear tracks were reconstructed by the equipped white-light interferometric profilometer. SEM images of the wear scar were obtained to analyze the wear morphology and type. The geometric parameters of wear scars (mm) and wear volume (V, mm^3) were obtained by white light interferometer data, and the specific wear rate (WR, $mm^3/(N \cdot m)$) was calculated according to Equation (2) that researchers mentioned [8,40].

$$WR = \frac{V}{Ps} \tag{2}$$

3. Results and Discussion

Figure 3 shows the fracture morphologies of SiC/SiC_w-Y_2O_3 composite ceramics obtained by the three-point bending tests. The porous microstructure can be observed in the Y000 and Y025 groups (Figure 3a,b), indicating their low compactness. As Y_2O_3 content increases, the number of pores on the fracture morphologies of the Y050, Y075, and Y100 groups is significantly reduced, and the connection between the grains becomes tight (Figure 3c–e). Thus, it can be concluded that the increased Y_2O_3 content can facilitate the compacting of SiC/SiC_w-Y_2O_3 composite ceramics. Besides, the embedded SiC_w and their pullout locations (yellow arrow) in the composite ceramics have also been pointed out. The SiC_w with high elastic modulus and low crystal defects can withstand the external force and not easy to generate the whisker fracture. The matrix fracture occurs when a high external force is applied and beyond the load-bearing capacity of the SiC matrix and SiC_w. During fracturing, when the external force exceeds the interface bonding force between SiC_w and SiC matrix, the SiC_w pullout phenomenon occurs [8,9].

To further reveal the microstructure characteristic of the compacted ceramic, the morphologies of Y075 and Y100 groups after careful polishing were observed by SEM (PDBSE mode), as shown in Figure 4a,b. The quantitative EDS was performed to estimate the Y_2O_3 content of the detected points with different grayscale areas, as shown in Figure 4b,c (for Y075) and Figure 4e,f (for Y100). It can be found that Y_2O_3 (area with lighter grayscale) filled in the gaps between SiC and SiC_w, proving that liquefied Y_2O_3 can promote particle rearrangement and mass transfer to increase the density during sintering [12,25,27]. In the Y075 group, Y_2O_3 is evenly distributed and presents a slender outline between the SiC and SiC_w. Sharma et al. [40] mentioned that the glassy phase distributed between the grain boundaries could enhance the fracture toughness by combining intergranular crack mode and energy-dissipating processes in the crack wake. In contrast, Y_2O_3 in the Y100 group shows severe aggregation. It can be predicted that excess Y_2O_3 aggregated around SiC and SiC_w may deteriorate the mechanical and relevant properties of the composite ceramics [26,27].

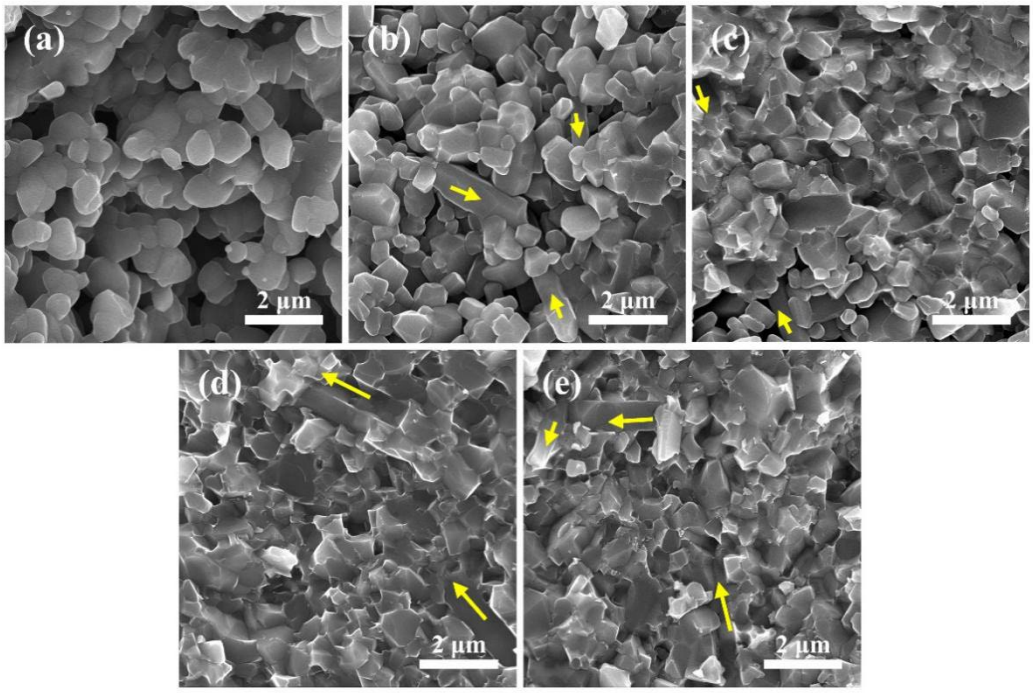

Figure 3. The fracture morphologies of SiC/SiC_w-Y_2O_3 composite ceramics with different Y_2O_3 contents. (**a**) Y000; (**b**) Y025; (**c**) Y050; (**d**) Y075; (**e**) Y100. The yellow arrow indicates SiC_w or its location after being pullout.

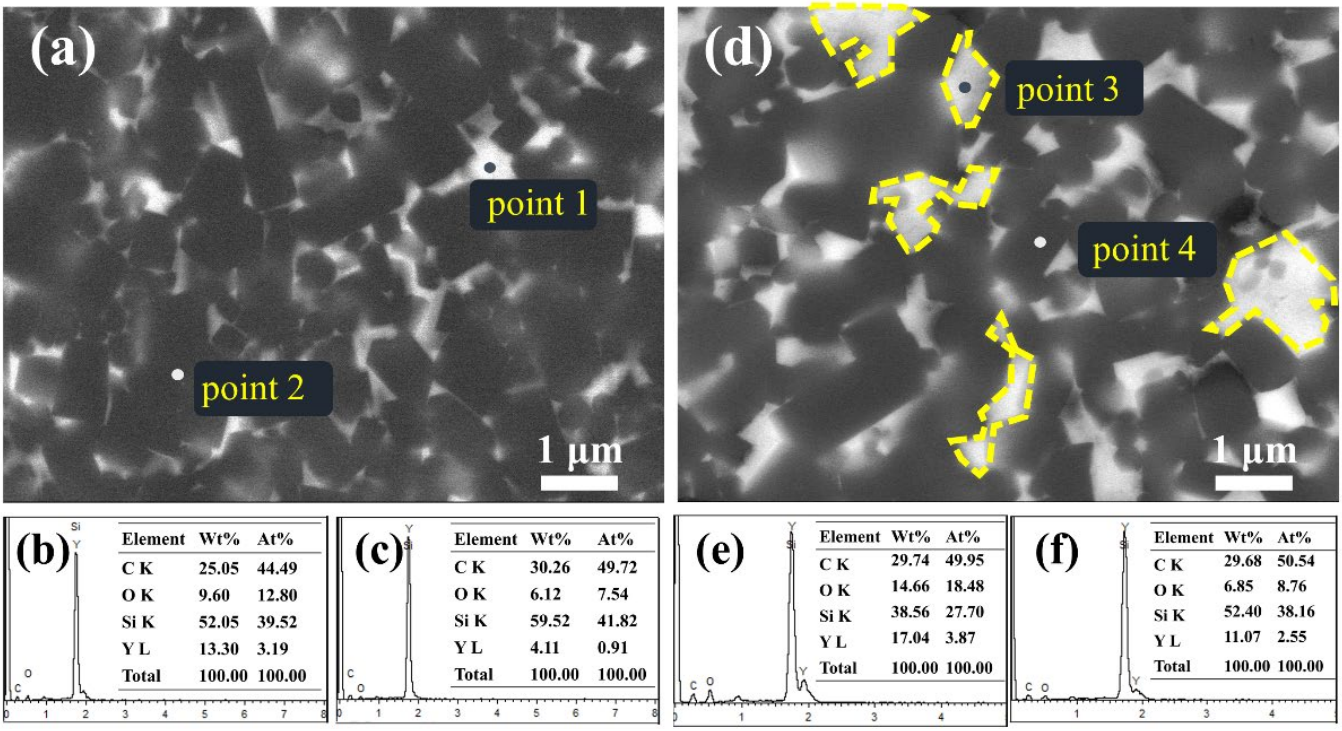

Figure 4. The PDBSE images and EDS point scan results of SiC/SiC_w-Y_2O_3 composite ceramics. (**a**–**c**) Y075, (**d**–**f**) Y100. Points 1 and 3 indicate the lighter grayscale area, and points 2 and 4 indicate the darker grayscale area on the polished morphologies.

XRD results are used to identify the phase composition of the SiC/SiC_w-Y_2O_3 composite ceramics, as shown in Figure 5. Most of the characteristic peaks of SiC can be detected (regardless of their specific crystalline structure) in all groups. The results in Figures 1 and 4 confirm the existence of SiC and SiC_w in the composite ceramics. Except for Y000, the

characteristic peaks (29.2° and 48.5°) belonging to PDF-#65-3178 can also be found in the rest groups, indicating the existence of Y_2O_3 in the composite ceramics. Moreover, the corresponding peak intensity of Y_2O_3 shows an increased trend with Y_2O_3 content increase. No new peaks and peaks shifting appear in the diffraction patterns, demonstrating the good stability of the three components during sintering.

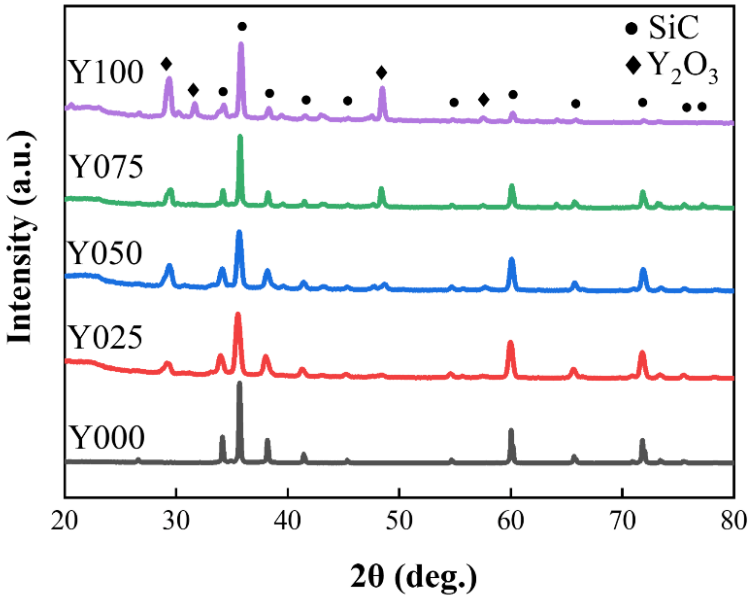

Figure 5. XRD patterns of SiC/SiC_w-Y_2O_3 composite ceramics with different Y_2O_3 contents.

The relative density, Vickers hardness, fracture toughness, and flexural strength of SiC/SiC_w-Y_2O_3 composite ceramics are shown in Figure 6. Figure 6a shows that the relative density of composite ceramic increases with Y_2O_3 content; Y000 has the lowest value of 54.3%. With Y_2O_3 content increase to 2.5 vol.%, 5 vol.%, 7.5 vol.%, and 10 vol.%, the relative densities reach to 87.6%, 91.5%, 97.0%, and 99.9%, respectively. The relative density results are consistent with the fracture morphologies shown in Figure 3, confirming that the addition of Y_2O_3 contributes to the compactness of the SiC/SiC_w-Y_2O_3 composite ceramics. It's worth noting that the poor compactness of Y000 reveals the formula failed when sintering in this process condition; therefore, many valid mechanical and tribological data cannot be obtained. For example, although the Vickers hardness of Y000 was obtained, it was only 1.3 GPa and at least an order of magnitude smaller than the other groups. Hence, the Y000 group was abandoned in subsequent tests. Compare the Y000 specimen with the other 4 groups containing Y_2O_3, confirming that Y_2O_3 additives have a noticeable promoting effect on the microstructure and mechanical properties of SiC composite ceramics. With the Y_2O_3 content increasing from 2.5 vol.% to 7.5 vol.%, the Vickers hardness increases from 10.9 GPa to 21.6 GPa, then decreases to 18.9 GPa when Y_2O_3 content is 10 vol.%. The results indicate that suitable Y_2O_3 content ($\leq$7.5 vol.%) can increase the Vickers hardness, and excessive Y_2O_3 content (10 vol.%) can weaken the Vickers hardness. Similar variations can be found in the fracture toughness (Figure 6c) and flexural strength results (Figure 6d). The values increase when Y_2O_3 content increases from 2.5 vol.% to 7.5 vol.% and then decrease when Y_2O_3 content reaches 10 vol.%. Of course, although the tested mechanical properties of Y100 are not the best, it is still slightly better than Y050 and Y025, proving that excessive Y_2O_3 does not significantly deteriorate the relevant performance dramatically. The hampered mechanical properties of Y100 are strongly affected by their microstructure since the aggregated Y_2O_3 can decrease its load-bearing capacity attributed to the poorer mechanical properties of Y_2O_3 compared with SiC [37]. Besides, the excessive Y_2O_3 made redundant liquid phase connect in a larger potential flaw fracture origin [26].

Seo et al. [19] reported the SiC-2 vol.%Y_2O_3 ceramic which was fabricated by hot-press sintering at 2000 °C, 40 MPa, N_2 for 3 h. The relative density, fracture toughness, and flexu-

ral strength are 99.1%, 3.4 MPa · $m^{1/2}$, and 586 MPa, respectively. SiC-2 vol.%Y_2O_3 ceramic shows slightly higher relative density and flexural strength than SiC/SiC_w-7.5 vol.%Y_2O_3 composite ceramic (Y075) sintered at 1800 °C in this study. Both studies indicate that Y_2O_3 can improve the densification of the as-sintered ceramics, and the SiC composite ceramics with an appropriate amount of Y_2O_3 can reduce the hot-pressed sintering temperature to a comparatively lower one (1800 °C). Furthermore, compared with Y075, the fracture toughness of SiC-2 vol.%Y_2O_3 ceramics decreased by 55.8%. It can be speculated that the SiC_w reinforced [6–9] and the Y_2O_3 pinned in [25] can both improve the mechanical properties, particularly the fracture toughness of the SiC composite ceramics. It can be concluded that incorporated Y_2O_3 and SiC_w can work together to improve the compactness of microstructure and the mechanical performance of the SiC composite ceramics.

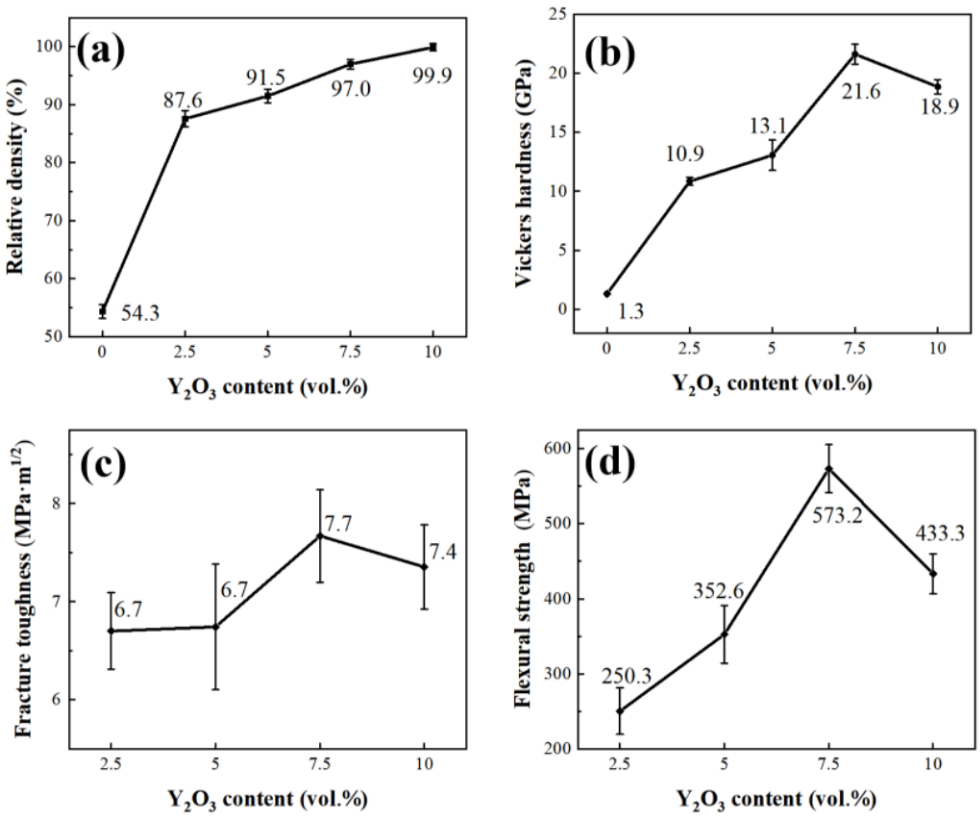

Figure 6. The variations of (**a**) relative density, (**b**) Vickers hardness, (**c**) fracture toughness, and (**d**) flexural strength of SiC/SiC_w-Y_2O_3 composite ceramics.

The COF variations of SiC/SiC_w-Y_2O_3 composite ceramics with sliding time are displayed in Figure 7a. In all groups, the COF sharply rises at the initial stage, then decreases and shows a relatively stable status after sliding for ~200 s. After contact with each other, the asperities on SiC/SiC_w-Y_2O_3 composite ceramic and YG6 ball increase the contact stress between them so that a considerable COF value can be obtained. After the run-in stage, the relatively stable COF indicates that the contact surface of the specimen and ball increases, indicating the decreased surface roughness of the grinding bodies. Although the COF at the stable stage does not change dramatically, slight increases of COF in groups with lower contents (Y025 and Y050) can still be seen. The average COF of Y025, Y050, Y075, and Y100 during the sliding period are 0.36, 0.35, 0.34, and 0.32, respectively, indicating that incorporating Y_2O_3 can decrease the COF of SiC/SiC_w-Y_2O_3 composite ceramics. Combined with the formula of SiC/SiC_w-Y_2O_3 composite ceramics, it can be boldly speculated that the worn Y_2O_3 debris can more easily fill the pits of the wear scars than SiC and SiC_w, reduce the roughness, and thus slightly reduce the COF. The COF and antifriction effect of Y_2O_3 is positively correlated with its content [37,40–42].

Figure 7b depicts the wear track profiles of SiC/SiC$_w$-Y_2O_3 composite ceramics. It can be seen both the width and depth of the wear track of composite ceramics decrease in groups with Y_2O_3 content ≤7.5 vol.%. As the Y_2O_3 content continues to increase, the width and depth of the wear track of Y100 increase, but it is still smaller than Y050. Besides, the wear scar profiles of Y075 and Y100 are smoother than Y025 and Y050, indicating the more compact microstructure and better mechanical properties of the latter groups. Figure 7c1–c4 vividly displays the 3D morphology of the wear track on each sample surface. These images exhibit the depth and width of the wear track (consistent with Figure 7b) and can reveal the surface roughness inside the wear track. As can be seen, the wear tracks of Y025 and Y050 possess larger roughness than Y100 and Y075, and the Y075 is the smallest. Generally, in the case of the same materials type, the smoother the surface, the lower the friction coefficient, and the better the wear resistance [43,44].

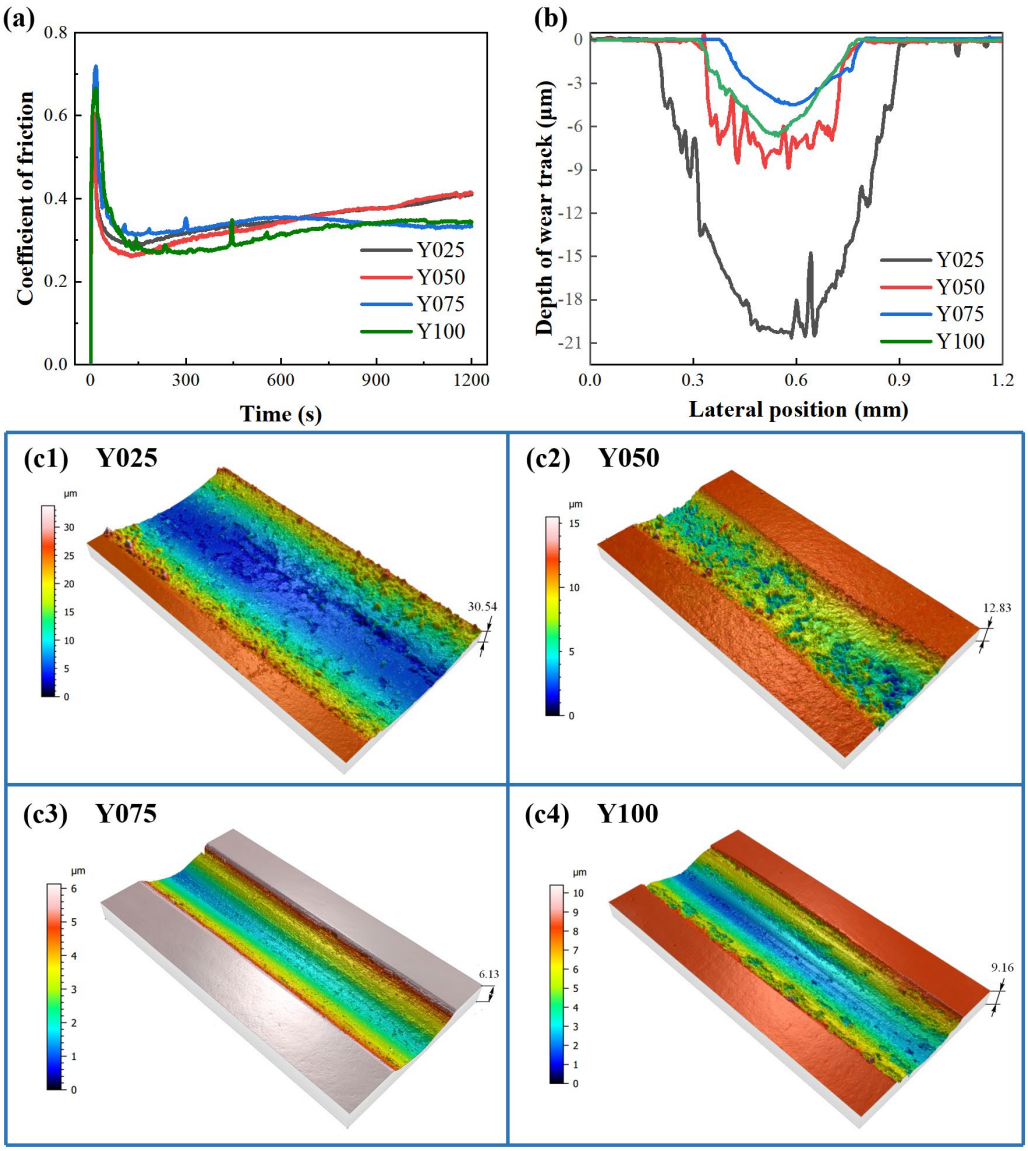

Figure 7. (**a**)The coefficient of friction, (**b**) the 2D, and (**c1–c4**) the 3D wear track profile of SiC/SiC$_w$-Y_2O_3 composite ceramics after grinding with YG6 balls at 20 N for 20 min: (**c1**) Y025; (**c2**) Y050, (**c3**) Y075, (**c4**) Y100.

The maximum depth, width, wear volume, and specific wear rate of the wear track of SiC/SiC$_w$-Y_2O_3 composite ceramics are listed in Table 1. The maximum depth and width are consistent with the results of 2D and 3D profiles in Figure 7b,c1–c4. Moreover, with Y_2O_3 content increasing from 2.5 vol.% to 7.5 vol.%, the wear volume and specific wear

rate reach the lowest value of 3.82×10^{-3} mm^3 and 1.59×10^{-5} mm^3/(N · m). As the Y_2O_3 content continues to increase, the wear volume and specific wear rate slightly increase but are still lower than the Y050 group. Thus, it can be concluded that high Y_2O_3 addition can reduce the COF, and Y_2O_3 additives can significantly improve the wear resistance of SiC/SiC$_w$-Y_2O_3 composite ceramics. SiC composite ceramics with 7.5 vol.%Y_2O_3 shows the best wear resistance than others.

Table 1. The maximum depth, maximum width, wear volume, and specific wear rate of the wear track of SiC/SiC$_w$-Y_2O_3 composite ceramics with different Y_2O_3 contents.

	Maximum Depth (mm)	Maximum Width (mm)	Wear Volume (mm^3)	Specific Wear Rate (mm^3/(N · m))
Y025	2.63×10^{-2}	7.30×10^{-1}	3.25×10^{-2}	1.35×10^{-4}
Y050	1.25×10^{-2}	5.01×10^{-1}	7.74×10^{-3}	3.23×10^{-5}
Y075	7.44×10^{-3}	4.09×10^{-1}	3.82×10^{-3}	1.59×10^{-5}
Y100	8.23×10^{-3}	4.51×10^{-1}	6.46×10^{-3}	2.69×10^{-5}

SEM images of wear scars reveal the correlation between the microstructure and wear resistance. As shown in Figure 8, the surface morphologies of wear scars (first line) are in accordance with the 3D profiles shown in Figure 7c1–c4. As for Y025, flaky debris does not connect tight in the microscale covered on the wear scar surface. This morphology was caused by the cold-welded debris onto the edge of the SiC. The flaky debris filled the holes of the hot-pressed ceramic, but due to the low friction heat and insufficient quantity, they do not have tight bonding with the substance below [43]. Meanwhile, the asperities bear greater friction and lead to worse wear resistance. The wear morphology and mechanism of Y050 are similar to that of Y025, but the wear surface of Y050 is mildly flat, and the wear resistance is improved over Y025 due to the increased relative density. Adding Y_2O_3 up to 7.5 vol.% and 10 vol.% further improves the relative density of composite ceramics, but excessive Y_2O_3 aggregated around SiC and SiC$_w$ (especially Y100) weakens the Vickers hardness and the subsequent wear resistance [27,45]. As seen in Figure 8c2,d2, no sintering holes exist in Y075 and Y100, but the size of cracks in Y100 is larger than in Y075, indicating poor mechanical properties of Y100. The lower hardness of Y_2O_3 than SiC is also responsible for the decreased wear resistance of Y100 [37]. Y075 group possesses the optimal wear resistance, and the abrasive wear plays an important role, as evidenced by smooth wear scar surfaces and long and thin furrows. The specific wear rate of Y075 is 11.8% than Y025.

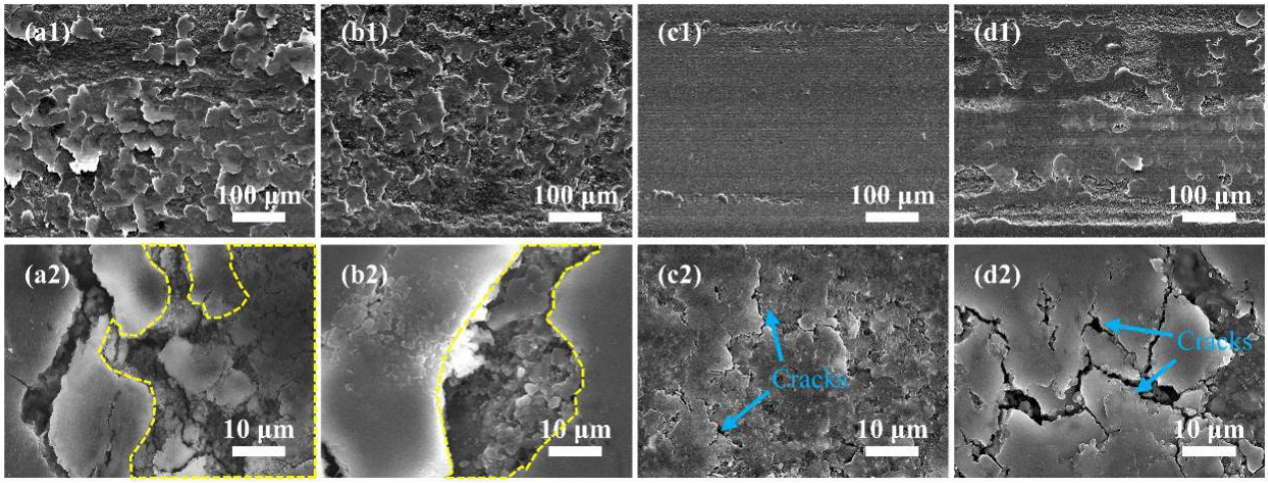

Figure 8. The SEM morphologies of the wear track of SiC/SiCw-Y_2O_3 composite ceramics with different Y_2O_3 contents. (**a1**,**a2**) Y025; (**b1**,**b2**) Y050; (**c1**,**c2**) Y075; (**d1**,**d2**) Y100. The yellow-dotted polygon outlines the sintering holes filled with wear debris.

4. Conclusions

SiC/SiC_w-Y_2O_3 composite ceramics with 10 vol.% SiC_w and different Y_2O_3 contents were fabricated by hot-pressed sintering at 1800 °C. The effects of Y_2O_3 content on the microstructure, mechanical properties, and tribological behaviors were systematically investigated. It is found that compact SiC/SiC_w cannot be hot-pressed without Y_2O_3 additives at 1800 °C and 40 MPa. With Y_2O_3 content increase, the microstructures are getting compact with increased relative density, but excessive Y_2O_3 leads to its aggregation. Moreover, with Y_2O_3 content increasing from 2.5 vol.% to 7.5 vol.%, the Vickers hardness, fracture toughness, and flexural strength all increase to the optimal values. As Y_2O_3 content increased to 10 vol.%, those properties were slightly reduced. Due to the compact microstructure, proper Y_2O_3 content, and excellent mechanical properties, SiC/SiC_w-7.5 vol.%Y_2O_3 ceramic (Y075) shows optimal wear resistance. The specific wear rate of Y075 is 11.8% of that for Y025 (SiC/SiC_w-2.5 vol.%Y_2O_3 ceramic). The excellent mechanical properties and good wear resistance of Y075 highlight its potential future application.

Author Contributions: Conceptualization, J.W. and L.Z.; methodology, S.Z. and J.W.; software, S.Z. and L.D.; validation, S.Z. and H.C.; formal analysis, X.L. and F.W.; investigation, Z.T., L.S. and S.C.; resources, L.Z.; data curation: S.Z.; data interpretation: S.Z. and S.D. writing—original draft preparation, M.Z., J.W. and S.Z; writing—review and editing, M.Z., J.W. and L.Z.; visualization, N.Y.; supervision, S.D.; project administration, L.Z. and S.C.; funding acquisition, L.S., N.Y. and L.Z. All authors have read and agreed to the published version of the manuscript.

Funding: The authors would like to acknowledge the National Natural Science Foundation of China (No. 21671145 and No. 52201187), the Zhejiang Province key research and development plan project (2023C01082), the General Scientific Research Project of Zhejiang Provincial Education Department (No. Y202249336), the Natural Science Foundation of Zhejiang Province (LQ19E050004), the Agricultural Science and Technology Key R & D Program of Taizhou (NYJBGS202201).

Institutional Review Board Statement: This article does not need ethical approval.

Informed Consent Statement: This article does not involve human experiments.

Data Availability Statement: Data are available from the corresponding author on reasonable request.

Conflicts of Interest: The authors declare no conflict of interest.

References

1. Xu, M.; Girish, Y.R.; Rakesh, K.P.; Wu, P.; Manukumar, H.M.; Byrappa, S.M.; Udayabhanu; Byrappa, K. Recent advances and challenges in silicon carbide (SiC) ceramic nanoarchitectures and their applications. *Mater. Today Commun.* **2021**, *28*, 102533. [CrossRef]
2. Padture, N.P. Advanced structural ceramics in aerospace propulsion. *Nat. Mater.* **2016**, *15*, 804–809. [CrossRef] [PubMed]
3. Kang, S.-J.L. What we should consider for full densification when sintering. *Materials* **2020**, *13*, 3578. [CrossRef]
4. Shimoda, K.; Hinoki, T. Effects of fiber volume fraction on the densification and mechanical properties of unidirectional SiCf/SiC-matrix composites. *J. Eur. Ceram. Soc.* **2021**, *41*, 1163–1170. [CrossRef]
5. Wei, C.; Zhang, Z.; Ma, X.; Liu, L.; Wu, Y.; Li, D.; Wang, P.; Duan, X. Mechanical and ablation properties of laminated ZrB_2-SiC ceramics with Si3N4 whisker interface. *Corros. Sci.* **2022**, *10*, 17003–17009. [CrossRef]
6. Li, S.; Zhang, Y.; Han, J.; Zhou, Y. Fabrication and characterization of SiC whisker reinforced reaction bonded SiC composite. *Ceram. Int.* **2013**, *39*, 449–455. [CrossRef]
7. Song, N.; Zhang, H.-B.; Liu, H.; Fang, J.-Z. Effects of SiC whiskers on the mechanical properties and microstructure of SiC ceramics by reactive sintering. *Ceram. Int.* **2017**, *43*, 6786–6790. [CrossRef]
8. Yang, Y.; Zhu, T.; Sun, N.; Liang, X.; Li, Y.; Wang, H.; Xie, Z.; Sang, S.; Dai, J. Mechanical and tribological properties of SiC whiskers reinforced SiC composites via oscillatory pressure sintering. *Int. J. Appl. Ceram. Technol.* **2023**, *12*, 1–12. [CrossRef]
9. Zhang, L.; Yang, H.; Guo, X.; Shen, J.; Zhu, X. Preparation and properties of silicon carbide ceramics enhanced by TiN nanoparticles and SiC whiskers. *Scr. Mater.* **2011**, *65*, 186–189. [CrossRef]
10. Kim, K.-J.; Lim, K.-Y.; Kim, Y.-W. Influence of Y_2O_3 addition on electrical properties of β-SiC ceramics sintered in nitrogen atmosphere. *J. Eur. Ceram. Soc.* **2012**, *32*, 4401–4406. [CrossRef]
11. Xie, W.; Fu, Q.; Cheng, C. Oxidation behavior of different La_2O_3-content modified SiC ceramic at 1700 degrees C. *Ceram. Int.* **2021**, *47*, 11560–11567. [CrossRef]
12. Tabata, S.; Hirata, Y.; Sameshima, S.; Matsunaga, N.; Ijichi, K. Liquid phase sintering and mechanical properties of SiC with rare-earth oxide. *J. Ceram. Soc. Jpn.* **2006**, *114*, 247–252. [CrossRef]

13. Liang, H.; Yao, X.; Zhang, J.; Liu, X.; Huang, Z. The effect of rare earth oxides on the pressureless liquid phase sintering of alpha-SiC. *J. Eur. Ceram. Soc.* **2014**, *34*, 2865–2874. [CrossRef]
14. Raju, K.; Yoon, D.-H. Sintering additives for SiC based on the reactivity: A review. *Ceram. Int.* **2016**, *42*, 17947–17962. [CrossRef]
15. Maity, T.; Kim, Y.-W. High-temperature strength of liquid-phase-sintered silicon carbide ceramics: A review. *Int. J. Appl. Ceram. Technol.* **2022**, *19*, 130–148. [CrossRef]
16. Strecker, K.; Ribeiro, S.; Oberacker, R.; Hoffmann, M.J. Influence of microstructural variation on fracture toughness of LPS-SiC ceramics. *Int. J. Refract. Met. Hard Mater.* **2004**, *22*, 169–175. [CrossRef]
17. Santos, A.; Ribeiro, S. Liquid phase sintering and characterization of SiC ceramics. *Ceram. Int.* **2018**, *44*, 11048–11059. [CrossRef]
18. Ge, S.; Yao, X.; Liu, Y.; Duan, H.; Huang, Z.; Liu, X. Effect of Sintering Temperature on the Properties of Highly Electrical Resistive SiC Ceramics as a Function of Y_2O_3-Er_2O_3 Additions. *Materials* **2020**, *13*, 4768. [CrossRef]
19. Seo, Y.-K.; Kim, Y.-W.; Kim, K.-J. Electrically conductive SiC-BN composites. *J. Eur. Ceram. Soc.* **2016**, *36*, 3879–3887. [CrossRef]
20. Zhu, Y.; Qin, Z.; Chai, J.; Shen, T.; Zhou, Y.; Wang, Z. Effects of sintering additives on microstructure and mechanical properties of hot-pressed alpha-SiC. *Metall. Mater. Trans. A* **2022**, *53*, 1188–1199. [CrossRef]
21. Lim, K.-Y.; Kim, Y.-W.; Kim, K.J. Mechanical properties of electrically conductive silicon carbide ceramics. *Ceram. Int.* **2014**, *40*, 10577–10582. [CrossRef]
22. Kueck, A.; Ramasse, Q.; De Jonghe, L.; Ritchie, R. Atomic-scale imaging and the effect of yttrium on the fracture toughness of silicon carbide ceramics. *Acta Mater.* **2010**, *58*, 2999–3005. [CrossRef]
23. Gao, J.; Xiao, H.; Du, H. Effect of Y_2O_3 addition on ammono sol–gel synthesis and sintering of Si_3N_4–SiC nanocomposite powder. *Ceram. Int.* **2003**, *29*, 655–661. [CrossRef]
24. Zhang, Y.; Yu, X.; Gu, H.; Yao, D.; Zuo, K.; Xia, Y.; Yin, J.; Liang, H.; Zeng, Y.-P. Microstructure evolution and high-temperature mechanical properties of porous Si3N4 ceramics prepared by SHS with a small amount of Y_2O_3 addition. *Ceram. Int.* **2021**, *47*, 5656–5662. [CrossRef]
25. Cheng, L.; Xie, Z.; Liu, J.; Wu, H.; Jiang, Q.; Wu, S. Effects of Y_2O_3 on the densification and fracture toughness of SPS-sintered TiC. *Mater. Res. Innov.* **2018**, *22*, 7–12. [CrossRef]
26. Zhang, X.; Li, X.; Han, J.; Han, W.; Hong, C. Effects of Y_2O_3 on microstructure and mechanical properties of ZrB2–SiC ceramics. *J. Alloys Compd.* **2008**, *465*, 506–511. [CrossRef]
27. Kováčová, Z.; Bača, Ľ.; Neubauer, E.; Kitzmantel, M. Influence of sintering temperature, SiC particle size and Y_2O_3 addition on the densification, microstructure and oxidation resistance of ZrB_2-SiC ceramics. *J. Eur. Ceram. Soc.* **2016**, *36*, 3041–3049. [CrossRef]
28. Aguirre, T.G.; Lamm, B.W.; Cramer, C.L.; Mitchell, D.J. Zirconium-diboride silicon-carbide composites: A review. *Ceram. Int.* **2022**, *48*, 7344–7361. [CrossRef]
29. Aguirre, T.G.; Cramer, C.L.; Cakmak, E.; Lance, M.J.; Lowden, R.A. Processing and microstructure of ZrB2–SiC composite prepared by reactive spark plasma sintering. *Results Mater.* **2021**, *11*, 100217. [CrossRef]
30. Li, W.; Zhang, X.; Hong, C.; Han, J.; Han, W. Hot-pressed ZrB2-SiC-YSZ composites with various yttria content: Microstructure and mechanical properties. *Mater. Sci. Eng. A* **2008**, *494*, 147–152. [CrossRef]
31. Serbenyuk, T.B.; Prikhna, T.O.; Sverdun, V.B.; Sverdun, N.V.; Moshchil', V.Y.; Ostash, O.P.; Vasyliv, B.D.; Podhurska, V.Y.; Kovylyaev, V.V.; Chasnyk, V.I. Effect of the additive of Y_2O_3 on the structure formation and properties of composite materials based on AlN-SiC. *J. Superhard Mater.* **2018**, *40*, 8–15. [CrossRef]
32. Wang, J.; Zuo, D.; Zhu, L.; Li, W.; Tu, Z.; Dai, S. Effects and influence of Y_2O_3 addition on the microstructure and mechanical properties of binderless tungsten carbide fabricated by spark plasma sintering. *Int. J. Refract. Met. Hard Mater.* **2018**, *71*, 167–174. [CrossRef]
33. Wang, J.; Zuo, D.; Zhu, L.; Tu, Z.; Lin, X.; Wu, Y.; Li, W.; Zhang, X. Effect of Y_2O_3 addition on high-temperature oxidation of binderless tungsten carbide. *Front. Mater.* **2021**, *8*, 645612. [CrossRef]
34. Liu, Y.; Li, X.; Zhou, J.; Fu, K.; Wei, W.; Du, M.; Zhao, X. Effects of Y_2O_3 addition on microstructures and mechanical properties of WC–Co functionally graded cemented carbides. *Int. J. Refract. Met. Hard Mater.* **2015**, *50*, 53–58. [CrossRef]
35. Hu, C.; Xiang, W.; Chen, P.; Li, Q.; Xiang, R.; Zhou, L. Influence of Y_2O_3 on densification, flexural strength and heat shock resistance of cordierite-based composite ceramics. *Ceram. Int.* **2022**, *48*, 74–81. [CrossRef]
36. Barick, P.; Chakravarty, D.; Saha, B.P.; Mitra, R.; Joshi, S.V. Effect of pressure and temperature on densification, microstructure and mechanical properties of spark plasma sintered silicon carbide processed with beta-silicon carbide nanopowder and sintering additives. *Ceram. Int.* **2016**, *42*, 3836–3848. [CrossRef]
37. Gupta, S.; Sharma, S.K.; Kumar, B.V.M.; Kim, Y.-W. Tribological characteristics of SiC ceramics sintered with a small amount of yttria. *Ceram. Int.* **2015**, *41*, 14780–14789. [CrossRef]
38. Guo, X.; Yang, H.; Zhang, L.; Zhu, X. Sintering behavior, microstructure and mechanical properties of silicon carbide ceramics containing different nano-TiN additive. *Ceram. Int.* **2010**, *36*, 161–165. [CrossRef]
39. Niihara, K.; Morena, R.; Hasselman, D.P.H. Evaluation of K_{IC} of brittle solids by the indentation method with low crack-to-indent ratios. *J. Mater. Sci. Lett.* **1982**, *1*, 533–538. [CrossRef]
40. Sharma, S.K.; Kumar, B.V.M.; Kim, Y.-W. Tribological behavior of silicon carbide ceramics—A Review. *J. Korean Ceram. Soc.* **2016**, *53*, 581–596. [CrossRef]
41. Kumar, B.V.M.; Kim, Y.-W.; Lim, D.-S.; Seo, W.-S. Influence of small amount of sintering additives on unlubricated sliding wear properties of SiC ceramics. *Ceram. Int.* **2011**, *37*, 3599–3608. [CrossRef]

42. Zhang, W.; Yamashita, S.; Kita, H. Progress in tribological research of SiC ceramics in unlubricated sliding-A review. *Mater. Des.* **2020**, *190*, 108528. [CrossRef]
43. Fischer, T.; Zhu, Z.; Kim, H.; Shin, D. Genesis and role of wear debris in sliding wear of ceramics. *Wear* **2000**, *245*, 53–60. [CrossRef]
44. Xia, H.; Qiao, G.; Zhou, S.; Wang, J. Reciprocating friction and wear behavior of reaction-formed SiC ceramic against bearing steel ball. *Wear* **2013**, *303*, 276–285. [CrossRef]
45. Cho, S.-J.; Um, C.-D.; Kim, S.-S. Wear and Wear Transition in Silicon Carbide Ceramics during Sliding. *J. Am. Ceram. Soc.* **1996**, *79*, 1247–1251. [CrossRef]